Hydrol. Earth Syst. Sci. Discuss., 6, 7439–7482, 2009
www.hydrol-earth-syst-sci-discuss.net/6/7439/2009/

Hydrology and Earth System Sciences Discussions

This discussion paper is/has been under review for the journal Hydrology and Earth System Sciences (HESS). Please refer to the corresponding final paper in HESS if available.

A comparison of ASCAT and modelled soil moisture over South Africa, using TOPKAPI in land surface mode

S. Sinclair and G. G. S. Pegram

Department of Civil Engineering, University of KwaZulu-Natal, Durban, South Africa

Received: 24 October 2009 – Accepted: 27 October 2009 – Published: 3 December 2009

Correspondence to: S. Sinclair (sinclaird@ukzn.ac.za)

Published by Copernicus Publications on behalf of the European Geosciences Union.

Abstract

In this paper we compare two independent soil moisture estimates over South Africa. The first estimate is provided by automated runs of the TOPKAPI hydrological model. The model has been adapted to run as a collection of independent 1 km cells located on a grid with a spatial resolution of 0.125°, using 3 hourly rainfall estimates and evapotranspiration forcing calculated at 1 h intervals.

The rainfall forcing used is the TRMM 3B42RT product, while the evapotranspiration forcing is based on a modification of the FAO56 reference crop evapotranspiration (ET_0), which accounts for vegetation health and the availability of surface and soil water, as limiting factors on the potential rate of evapotranspiration.

We compare the ET_0 estimates, computed using observed meteorological data at a network of weather stations, to those computed using 24 h forecast fields from the South African Weather Service's Unified Model runs. The results show that the ET_0 computed using the forecast fields is strongly correlated with and unbiased relative to, the independent values computed (from observed data) at the weather station locations. We therefore conclude that the Unified Model forecasts are suitable for producing an estimate of ET_0 instead of observed station data, especially considering the sparse coverage of weather stations in the region.

Using the rainfall and evapotranspiration forcing data, the percentage saturation of the TOPKAPI soil store is computed, for each of 6984 uncalibrated TOPKAPI cells at 3 h time-steps, and compared with estimates of surface soil moisture from the ASCAT instrument onboard the METOP polar orbiter. The comparisons indicate a good correspondence in the dynamic behaviour of an exponentially filtered time series of the ASCAT surface soil moisture and the TOPKAPI estimates for several climatic regions in South Africa. The linear agreement in dynamic behaviour for these independent soil moisture estimates suggests that both are correctly capturing the soil moisture dynamics for a significant proportion this region, and could be combined to produce a "best estimate" soil moisture field.

HESSD

6, 7439–7482, 2009

1 Introduction

Up-to-date estimates of soil moisture are of interest across a wide range of disciplines, including numerical weather prediction, agricultural applications and flood modelling. The current soil moisture state is a good indicator of flash flood potential on small catchments with a short response time but is not easily measured. There is significant global interest in estimating soil moisture from satellite platforms (e.g. Wagner et al., 1999; Njoku et al., 2003; Kerr et al., 2001). One of the major challenges facing providers of soil moisture products is validation. This is mainly due to the limited availability and coverage of in situ observation networks (Albergel et al., 2009). Several authors have pursued alternative techniques of validation, inter alia correlations between river flows and soil wetness (Scipal et al., 2005) and assimilation of remotely sensed soil moisture estimates into a water balance model (Crow, 2007).

One outcome, of a current South African Water Research Commission funded project on soil moisture estimation, is an automated modelling system that produces country-wide estimates of soil moisture state at a 3 h time-step on a 0.125° spatial grid over South Africa. The key focus of this product is to provide a proof of concept for operational use by the South African Weather Service in their national Flash Flood Guidance (FFG) system, which will be an implementation of the system described by Ntelekos et al. (2006). There are numerous other fields (other than FFG) such as crop modelling, and drought monitoring where soil moisture estimates could prove beneficial.

In this paper, we describe a soil moisture modelling process, which includes a technique for determining reference crop evapotranspiration (ET_0, Allen et al., 1998) using forecast fields of meteorological variables from a numerical weather prediction model, run operationally be the SA Weather Service (SAWS, see Sect. 2). We continue by presenting an overview of the soil moisture modelling system (Sect. 3), which is based on a local implementation of the TOPKAPI hydrological model (Liu and Todini, 2002; Vischel et al., 2008a,b) adapted to run in Land Surface Modelling (LSM) mode. In

HESSD
6, 7439–7482, 2009

Sect. 3 we also present some examples of the soil moisture simulations produced by the TOPKAPI-LSM model, while in Sect. 4 we describe a remote sensing soil moisture retrieval product (Bartalis et al., 2008) from the ASCAT instrument onboard EUMETSAT's METOP polar orbiting satellite. In that section we also present and discuss the results of comparisons made between the two independent soil moisture estimates at selected locations in South Africa. In Sect. 5 we investigate possible reasons for the poor correspondence found in some parts of the country, while in Sect. 6 we draw conclusions based on the results presented in the paper.

2 Estimation of evapotranspiration

Evapotranspiration is widely accepted as an important component in the water balance at a range of different space and time scales but is difficult to measure directly over large areas at frequent time intervals (e.g., McCabe and Wood, 2006). This is particularly important in Southern Africa, where a large proportion of the rainfall is lost through evaporative processes, resulting in a country-wide runoff/rainfall ration in the order of 10%. Since evapotranspiration is driven by the surface energy balance (Eq. 1), its spatial distribution is determined by the spatial behavior of the components of this energy balance and can therefore be quite complex (particularly at detailed space and time scales). The surface energy balance on a control volume, including the surface vegetation and the first few centimeters of soil, can typically (e.g., Su, 2002) be written as a scalar equation:

$$R_n = \lambda ET_a + H + G \quad (1)$$

where R_n is the net radiation flux into the control volume, H is the sensible heat flux out of the control volume into the air stream, G is the heat flux out of the control volume into the ground, ET_a is the actual evapotranspiration from the control volume to the air and λ is the latent heat of vaporization of water.

HESSD
6, 7439–7482, 2009

As part of a South African Water Reasearch Commission funded project, focussed on soil moisture estimation in Southern Africa (using land surface modelling and remote sensing), a spatial grid of reference crop evapotranspiration estimates (ET_0) is routinely produced using the methodology described in Allen et al. (1998). ET_0 can be related to ET_a through the application of location and season dependent land cover and water stress coefficients. The approach taken here is detailed in Sect. 2.4.

Forecasts (24 h ahead) of the meteorological variables required for ET_0 estimation are obtained from the SAWS Unified Model (UM) runs, from which an hourly estimate of ET_0 is computed for each model grid cell. The resulting ET_0 estimates are produced on a 0.11° grid, matching that of the UM. This ET_0 product is used as forcing data for a distributed hydrological model, which is used to compute distributed estimates of soil moisture (Sect. 3).

2.1 Description of data sources

This section describes the sources of data used to produce and validate the spatially distributed ET_0 estimates.

2.1.1 Automatic Weather Station Network

The SAWS Automatic Weather Station (AWS) network provides surface meteorological information to a central data-collection facility. The network is shown in Fig. 1, indicating the relatively sparse coverage over the country (164 stations in 1.2 million km^2). Due to this sparse coverage the weather stations are not used as the sole source of information for producing spatial ET_0 estimates, as they are unable to efficiently sample the spatial detail of the meteorological fields. We use them to make comparisons with the estimates we obtain from the UM forecasts, with which they are shown (Sect. 2.3) to be unbiased and relatively highly correlated.

The meteorological variables measured at each station which are relevant to the computation of ET_0 are: temperature, relative humidity and wind speed. No radiation measurements are made at these stations, an alternative was sought – see Sect. 2.1.3.

HESSD
6, 7439–7482, 2009

2.1.2 Unified model

SAWS has recently (late 2006) installed the UK Met Office's UM, which is run at a grid resolution of 0.11° with 401 rows and 601 columns, covering Africa and the surrounding oceans south of the Equator. The bounding co-ordinates of the grid are defined by 10° W to 56° E and 0° S to 44° S, this region is shown on a square Latitude-Longitude grid in Fig. 2. The model is run twice daily in a number of different configurations. Assimilation of observed data and boundary conditions occur at 00:00 UTC and 12:00 UTC, and hourly weather forecasts are produced out to 48 h from each model run time. The model fields used in this study are the 00:00 UTC analysis fields and the corresponding forecast fields out to 23 h ahead.

2.1.3 Solar radiation

Because it is difficult to find operational surface radiation observations at an hourly (or even daily) frequency in South Africa, solar radiation estimates based on Meteosat data were selected. The data products are obtained from the Land Surface Analysis Satellite Application Facility (LSA-SAF http://landsaf.meteo.pt) and are disseminated in real time at 30 min intervals via the EUMETCast system, which we download in real-time to our server, under a research agreement with EUMETSAT.

The advantage of this product, in comparison to sparse surface AWS observations, is that a detailed spatial coverage is available over large areas at frequent intervals. Figure 3 shows a typical map of the estimated solar radiation flux for Africa, South of the equator. Clouds are clearly implied, in areas coloured green through to blue, indicating various degrees of radiation occlusion.

To the best of the authors' knowledge, the LSA-SAF DSSF product has only been validated under European conditions, (LSA-SAF, 2006) where it was shown to be unbiased, and its applicability in Southern Africa was not known before this study, but similar results were a reasonable expectation. As an exercise to increase confidence in the estimates, a basic comparison with some observed data was carried out.

A time series of solar radiation data collected from the CSIR study catchments (30.67° S, 29.19° E), situated at the Mistley-Canema Estate (Mondi Forests) in the Seven Oaks district, approximately 70 km from Pietermaritzburg was obtained (C. Everson, 2008, personal communication). These observed data were compared with the LSA-SAF estimates at the same location and times. Figure 4 shows a comparison between the measured and estimated solar radiation over a period of 5 days between 20 and 24 February 2007. This initial test of applicability is very encouraging, with the coefficient of determination (R^2) for the best fit linear regression line equal to 0.918.

2.2 Methodology for computing ET_0 from meteorological variables

It is difficult to solve the Surface Energy Balance directly for ET_a without directly measuring all of the radiative fluxes (for an example of the complexities of detailed measurements see Savage, 2009; Savage et al., 2009), so the estimation at each UM grid point uses the Penman-Monteith equations recommended in FAO56 (Allen et al., 1998). The result is an estimate of evapotranspiration for a well watered (sufficient soil water to meet maximum demand) reference crop defined as

> *A hypothetical reference crop with an assumed crop height of 0.12 m, a fixed surface resistance of 70 s m^{-1} and an albedo of 0.23* – Allen et al. (1998)

An implementation of the hourly algorithm described in Allen et al. (1998) has been developed for this study using the Python programming language. This code has been applied to process SAWS model (and station) data and produces an estimate of ET_0 at each grid point in hourly increments. The hourly estimates of ET_0 (an example is shown in Fig. 5) can be summed to produce a daily total, an example of which appears in Fig. 6, for illustration purposes, although we use 3 hourly evapotranspiration to force the TOPKAPI-LSM soil water calculations.

The FAO56 "reduced form" Penman-Monteith equation applied to the surface control volume is given in Eq. (2) below:

$$ET_0 = \frac{0.408\Delta(R_n - G) + \gamma \frac{C_n}{T+273} u_2 [e_s - e_a]}{\Delta + \gamma(1 + C_d u_2)} \quad (2)$$

where Δ is the slope of the saturation vapor pressure versus temperature curve, R_n is the net radiation influx, G is the soil heat flux, γ is the pyschrometric constant, T is the temperature, u_2 is the wind speed at 2 m height, e_s is the saturation vapor pressure, e_a is the actual vapor pressure. The coefficients C_n and C_d vary with the aerodynamic and bulk surface resistance and are therefore specified according to the calculation time step, reference surface type (grass in this case) and, as suggested by Allen et al. (2006), the time of day.

The meteorological data required to evaluate Eq. (2) (using Allen et al., 1998) are: air temperature, relative humidity, wind speed and solar radiation; the detail of the calculations is not repeated here as it is well known and can be found in Allen et al. (1998).

2.3 Spatially distributed estimates of evapotranspiration

Using the UM forecasts of meteorological variables on the model grid, ET_0 values are calculated in hourly time-steps for each model grid point, for a subset of the SAWS UM domain. In Fig. 5 a typical map of ET_0 calculated at an hourly time step is shown. In this case (12:00 SAST, or 10:00 UTC) a 10 h ahead forecast of the meteorological variables has been used together with the corresponding LSA-SAF radiation estimate, using Eq. (2). A linear regression through the origin between the two ET_0 estimates is shown in Fig. 7. The regression compares the ET_0 computed from observations at each station in the SAWS automatic weather station network (Fig. 1) to the ET_0 computed at the nearest UM grid point in the map shown in Fig. 5. Since it is well known that the R^2 value is reduced for regressions through the origin (Gordon, 1981) and is in fact disputed as a measure of the goodness of fit by some (Eisenhauer, 2003),

the Pearson correlation coefficient is also given for comparison. The R^2 of 0.78 and Pearson correlation coefficient of 0.90 both indicate a strong correspondence between the model forecast and station-based ET_0, while the slope of the regression indicates a lack of bias since it is close to one.

The map of daily ET_0 shown in Fig. 6 is produced by summing the hourly estimates (e.g. Fig. 5) over a 24 h period. The hourly ET_0 computed from the SAWS station observations have also been accumulated to daily totals and these are compared to the spatial estimates in the same way as was done to produce Fig. 7. The strong correlations between the station and spatially distributed ET_0 estimates (at the station locations) indicate that the spatial estimates based on Unified Model forecasts reproduce the ET_0 well at many locations throughout South Africa and also identify some ground based data which are clearly in error.

2.4 Obtaining an estimate of actual evapotranspiration

Having developed a technique to estimate grass reference evapotranspiration (ET_0) using the Penman-Monteith formulation of FAO56, we needed a means of utilizing this information on a day-by-day basis to obtain actual evapotranspiration (ET_a) in a way that adjusts according to dynamic changes due to vegetation health and water availibility for evaporation and transpiration.

In our implementation of the TOPKAPI model we chose to use water stress and a crop factor to modify ET_0 (e.g. Allen et al., 1998) and model ET_a as shown in Eq. (3)

$$ET_a = K_s K_c ET_0 \tag{3}$$

where K_s is a water stress co-efficient between 0 and 1 (we use a direct linear relationship with the degree of saturation in the soil store), and K_c is a co-efficient dependent on vegetation health and the available water at the soil surface.

Tasumi et al. (2005) suggest that NDVI is a good surrogate for K_c, as long as the vegetation is fairly well developed and transpiring. We adapted their formulation to allow for evaporation from wet soil when vegetation (hence NDVI) was low. Tasumi

et al. (2005) give the derived relationships between K_c (which they define as the ratio ET_a/ET_0; for irrigated crops i.e. $K_s = 1$) and NDVI. Their work defines a basal K_{cb} relationship that, if used by itself, produces a progressively smaller K_c as NDVI (vegetation cover) reduces. In addition, they show that for very low NDVI, K_c can vary from 0 to 1, which is interpreted to be the evaporation from wet bare soil. The K_{cb} curve behaves as expected for values of NDVI above 0.6, but below that one needs to allow for wet soil evaporation.

We compute a first estimate of K_c using the K_{cb} base-line and adjust this to accommodate a wet bare soil when vegetation is sparse and not actively transpiring. The formulation we adopted was the concept of a virtual store EV which we call the "available water for evapotranspiration". We allow EV to experience carry-over during a rainy period using a simple correlation R, modified with a limited amount of rainfall (it cannot exceed ET_0) with up to ET_0 being removed on the previous day. The ET_a on the current day cannot exceed the value of EV nor $K_c ET_0$ if there is well developed vegetation. The formulation is as follows, enabling us to calculate ET_a for each 3 h model time-step:

$$\begin{aligned} EV_i &= \min(ET_0, \max(R * EV_{i-1} + \min(\mathrm{RAIN}_i, ET_0) - ET_0, 0)) \\ ET_a^i &= K_s \max(EV^i, K_c ET_0) \end{aligned} \quad (4)$$

where RAIN_i is the rainfall estimate at the current time-step.

In summary, the formula allows evaporation of some of the rainfall up to a maximum of the current ET_0 at times when there is no vegetation and also allows removal of soil water by active vegetation as soon as NDVI dominates.

3 Soil moisture modelling using TOPKAPI in LSM mode

The TOPKAPI model code has been adapted to allow it to be operated as a collection of independent cells. Each model cell has a plan area of 1×1 km and the cell centres are located on a regular latitude and longitude grid with a grid spacing of 0.125°. The

model parameters (soil properties, slopes, land-use characteristics) have been determined for each cell, based on several static datasets and primarily using the methods described in Vischel et al. (2008a). The rainfall forcing applied is the real-time TRMM 3B42RT product (Huffman et al., 2007), which is automatically downloaded from the NASA server and processed locally. The ET_a forcing is based on a modification of the FAO56 (Allen et al., 1998) reference crop evapotranspiration (ET_0), accounting for vegetation state and the availability of both surface and soil water to meet the evaporative demand (as described in Sect. 2.4). The technique we developed to estimate ET_a from ET_0, NDVI and rainfall, turns out to be very similar to the methodology developed by Guerschman et al. (2009).

The TOPKAPI-LSM simulations are run once daily with a 3 h time step and the results archived. Figure 8 shows a snapshot of the computed SSI state for 00:00 UTC 18 December 2008. The colour scale ranging from brown to blue indicates the Soil Saturation Index (SSI) as a percentage, with light grey indicating regions where no modelling was carried out. The SSI is defined as the percentage of soil void space taken up by water

$$\mathrm{SSI} = 100\left(\frac{\theta}{\theta_s - \theta_r}\right) \tag{5}$$

where θ is the soil moisture content, θ_s is the saturated moisture content and θ_r is the residual moisture content.

4 Inter-comparison of TOPKAPI and ASCAT

In the absence of in situ soil water data available routinely in enough detail, inter-comparisons between the TOPKAPI modelled SSI and a remote sensing soil moisture retrieval have been carried out. This section describes the remote sensing based soil moisture product, the method used in the comparisons, and presents selected results and discussion.

4.1 ASCAT surface soil moisture

The advanced scatterometer (ASCAT) instrument onboard the polar orbiting METOP satellite is an active microwave instrument that measures backscatter from terrestrial surfaces. The backscatter signal measured by ASCAT is strongly influenced by the water content of soil, since the soil dielectric constant increases with increasing water content (Wagner et al., 2007). In this study we considered the 25 km ASCAT soil moisture product, which is available on a 12.5 km grid with orbit geometry.

The ASCAT retrieval is a change detection method, with the current backscatter measurement being scaled between wet and dry backscatter limits for each location in order to produce a relative soil moisture value (Bartalis et al., 2008). This surface soil moisture (SSM) value can be interpreted in terms of soil moisture content if the soil properties (saturated and residual moisture contents) are known for the location. In this study we have only considered the SSM since it is most similar to the TOPKAPI-LSM SSI that we compute. This premise is, based on the assumption made by Bartalis et al. (2008), that the wet and dry backscatter limits have been computed from a time series that contains at least one observation where the soil was at it's saturated moisture content (as well as at least one observation where the soil was at it's residual moisture content).

Figure 9 shows the SSM from a typical METOP overpass. The overpass is eight hours later than the TOPKAPI-LSM SSI estimates shown in Fig. 8. The SSM values are clearly lower than the SSI values in general and although there are similar spatial patterns evident, these are not easily discernible without normalizing the values. It is only after low pass filtering of the SSM signal in time (to remove the temporally most noisy portion of the signal), that stronger correspondence between the two estimates emerges (see Sect. 4.2–4.4).

4.2 Method of comparison

Due to the different spatial and temporal sampling of the ASCAT and TOPKAPI based soil moisture estimates, it was difficult to make any objective comparisons without first resampling one or both of the data sets. In order to begin developing a detailed understanding of the properties of the two estimates, we chose the following approach. First, we selected four different regions of South Africa using the work of Pfeffer (2008). The site selection was largely based on differences in vegetation type and Mean Annual Precipitation (MAP). Figure 10 shows the locations labelled A through D, plotted on a representation of MAP derived from the WR90 dataset (Midgley et al., 1994).

Soil moisture estimated by TOPKAPI and ASCAT was aggregated over 0.25° and 0.5° blocks (at locations A–D) for each of the four climatic regions during the 5 month period from August to December 2008. The data are plotted in Figs. 11–14 (discussed in the next section), no attempt was made to resample temporally.

Since the ASCAT retrieval is only sensitive to surface soil moisture changes (<5 cm depth), the values change rapidly and appear quite noisy. Following the work of Wagner et al. (1999), we choose to apply an exponentially weighted time filter to extract the low frequency signal from the spatial mean of the ASCAT retrievals in each block. The expectation was that this would be more representative of the soil moisture state in deeper soil layers, due to smoothing of the near surface signal by the infiltration processes. The SSI computed from TOPKAPI is a representative average condition of the entire A and B soil horizon, which varies in depth by location.

The initial value of the filter was chosen to be the first available block mean ASCAT soil wetness and the filter's time constant was set at 20 days (Wagner et al., 1999). The filter used is described as

$$y_t = (1-\alpha)y_{t-1} + \alpha x_t; \qquad \alpha = \Delta t / k \tag{6}$$

where y_t is the current filtered value of the time series, y_{t-1} is the previous filtered value, x_t is the current value of soil wetness, Δt is the time-step (variable, typically 2–3 days) between estimates and k=20 days is the time constant of the filter. We use the

HESSD
6, 7439–7482, 2009

approximation: $1-\alpha \approx \exp(-\alpha)$, which is good when $\alpha < 0.15$. Both the raw and filtered ASCAT estimates for each block size were then compared to the equivalent closest (in time) TOPKAPI-LSM SSI by means of linear regressions, with the R^2 of the regression used as a criterion to determine the "goodness of fit".

Such an analysis was carried out for a grid of 0.25° blocks covering the region. Linear regressions were calculated between the mean TOPKAPI SSI and ASCAT SSM on each block and the R^2 values are plotted on Fig. 16 for both raw ASCAT block mean and the time filtered ASCAT block mean SSM, in the upper and lower panels respectively.

4.3 Results of comparison

In this section, selected illustrative results of the comparison are presented. The first set of figures (Fig. 11 through 14) show the time series of soil moisture estimated in each of the four different climatic regions over either 0.25° or 0.5° blocks during the 5 month analysis period running from 1 August 2008 to 31 December 2008. The top panel in each figure shows the block median TOPKAPI-LSM SSI estimate as a blue line, with the inter-quartile range indicated by the grey shaded region. The box and whisker plots show the range of ASCAT SSM estimates within each block. The red line shows the exponentially weighted filter applied to the block mean value of the ASCAT estimates. The bottom panel shows 3 h rainfall accumulations estimated by TRMM 3B42RT.

Figures 11–14 show a selection of the results for a number of different configurations with the following characteristics: i) ascending, descending and combined (both) METOP orbit directions; ii) either 0.25° or 0.5° block averaging; iii) cases where SSI and SSM are well/poorly correlated. We note that there is a wide scatter between the ASCAT estimates, both on a given overpass/day and also between passes. In fact there is a clear 29 day periodicity evident in the ASCAT data shown in Fig. 14, for the Western Cape site. This period matches the 29 day repeat cycle of METOP (Figa-Saldaña et al., 2002). We therefore explored the nature of the ASCAT observations

to attempt to explain the behaviour and understand the error structures. This will be discussed in Sect. 5.

It turns out that, after exponential filtering the ASCAT data with the simple AR(1) (Eq. 6), the relationship for 3 of the sites is nearly linear and highly correlated. Figure 15 shows scatter plots of the block mean TOPKAPI-LSM soil moisture against the block mean unfiltered (left-hand panels) and filtered (right-hand panels) ASCAT soil moisture series. These two examples illustrate the effect of the exponential filter in removing the high frequency variability from the ASCAT time series.

Figure 16 shows two maps of the coefficient of determination (R^2) for the linear regression computed between block averaged SSI and SSM on 0.25° blocks covering the region. The top panel shows the R^2 values computed, based on the unfiltered time-series of SSM, while the bottom panel shows the results based on the filtered time-series.

4.4 Discussion of results

As shown by the box and whisker plots in Figs. 11–14, the ASCAT SSM shows a high variability both within each block and in time. This behaviour is expected since the near surface (0–50 mm) soil moisture will either evaporate or infiltrate into deeper soil layers within a fairly short space of time. The ASCAT SSM does increase in response to most rainfall events, for example there is a clear increase due to rainfall in mid-August and early October shown in Fig. 11. Overall, the high variability of the raw ASCAT SSM estimates results in a poor correlation with the TOPKAPI SSI simulations (left-hand panels of Fig. 15 and top panel of Fig. 16) if they are not filtered to reduce the effect of the noise.

The filtered SSM shows a much stronger link to the SSI estimates for all locations, except the Western Cape's behaviour displayed in Fig. 14, where the 29 day periodicity is highlighted by green dots (location A in Fig. 10). This correspondence is shown both in terms of the general trend and in the response to individual rainfall events when comparing the red and blue lines in Figs. 11–14 and the improved regressions in Fig. 15

(right panels) and 16 (lower panel). There are some notable exceptions to this trend, which we can not yet explain. The first exception is found in mid-October, where the ASCAT SSM response after the rainfall event in Fig. 13 (Crocodile catchment) is lower than expected given the surrounding observations and as a result the filtered SSM is lower. Another exception is that the SSM estimates are climbing during August on the Liebenbergsvlei (Fig. 12), when there appears to be no rain. In this case we can offer some possible explanations i) the TRMM rainfall product may have failed to detect rainfall that occurred during that period ii) the soil moisture may have been increasing due to the effects of irrigation or groundwater, which are not captured by the TOPKAPI modelling process.

Figure 16 shows that the TOPKAPI SSI and ASCAT SSM estimates are generally well correlated in the more densely populated and wetter eastern regions of South Africa, while the arid central western regions (which are understandably sparsely populated) show poor correspondence. In places where the correspondence is good (high R^2) it seems reasonable to suggest that both modelled and remote sensing estimates are correctly responding to the true soil moisture dynamics. In the regions of poor correspondence (low R^2), it's unclear which (if any) of the estimates is producing credible information on the changes in soil moisture conditions. Additional information is required to resolve this problem, in the form of in situ measurements and alternative independent estimates for further corroboration.

The maps in Fig. 16 are summarized in Fig. 17, which shows the percentage of 0.25° blocks with an R^2 equal to or greater than the value indicated on the x-axis. The figure shows the dramatic increase in R^2 from raw (unfiltered) ASCAT to filtered ASCAT SSM. As an example, it can be inferred from the figure (see green dashed lines) that 50% of the region has $R^2 >= 0.52$ for the filtered SSM, while in the unfiltered case 50% show $R^2 >= 0.08$. There is also a large difference in the maximum R^2 values.

5 Error structures

The high variability and the 29 day repeat cycle of the ASCAT observations prompted us to look more closely at the data. The SSM estimates from ASCAT for a given overpass are collected in two swaths, one East the other West of the METOP path (Naeimi et al., 2009). Figure 9 shows the estimate for the downward pass on 18 December 2008. In addition to the soil moisture estimates, the data includes an error estimate for each location in units of SSM %, as shown in Fig. 18. This error estimate, due to instrument noise, speckle and azimuthal effects, is calculated from the standard deviation of the backscatter difference between the fore and aft antennas and propagated through the calculation procedure to give an error estimate in SSM % (Bartalis et al., 2008). Understandably, there are larger errors at the coast and over the mountainous and forested areas of the Southeast (Cape) and the Northeast (Mpumalanga). Surprisingly, given the behaviour of the box-plots in Fig. 14, the error structure shown in Fig. 18 does not appear to depend on the incidence angle of the C-band, shown in Fig. 19 for the middle antenna; note that the incidence angle varies from 25 to 53° across the swath.

In Fig. 20, we have chosen a 0.5° square site near our Western Cape site (A in Fig. 10) and recorded the positions of the reported centres of the observations by ASCAT over a five-day period. We found that there were 3 upward (from South to North) passes and one downward pass in the chosen period. The top-left panel shows the collection of estimates over the site, suggesting SSM values between 0 and 30 % and the top-right panel gives the estimated errors distributed with the ASCAT product. To interpret these estimates, the bottom right panel shows the order in which the passes occurred: 1st deep blue (upward), 2nd lime green (upward), 3rd yellow (downward) and 4th brown (upward).

It is reassuring that the observations and the errors tend to cluster by colour, however a deeper look indicates that the light pink (20 to 30%) estimates are those of the 3rd (downward) pass and are locally outliers in the T-shaped area, but agree with the other

HESSD
6, 7439–7482, 2009

observations in the Southwest and Southeast patches of dryness. The rainfall records show that there was no rain in this period.

Following on from the analysis displayed in Figs. 18 and 20, we collected all the errors in each 0.25° square over the 5 months of our study period. These were averaged over each block and averaged over time. The results appear in Fig. 21, where the effect of the eastern coastline and the associated coastal forest will be seen in green. Most of the remainder of the country averages out at a remarkably small 1 to 2%, with the exception of the known mountainous regions.

This image contrasts starkly with Fig. 22 which, appears in Bartalis et al. (2008) and is based on ERS data. This figure, on closer scrutiny over Southern Africa, indicates substantial errors (5 to 7%) in the Western half of South Africa and smaller (2 to 3%) errors over the Eastern half. This pattern agrees broadly with the map of correlations between SSM and SSI estimates that we display in Fig. 16.

We cannot explain the anomaly, but favour the correspondence of our results with (this) Fig. 22, rather than Fig. 21, given the poor results displayed by ASCAT for the Western Cape (Fig. 14).

The results of the comparisons are very encouraging over half of South Africa. However, we have not yet been able to determine the cause of the discrepancies in the remaining areas.

6 Conclusions

In this paper we have introduced an automated approach to modelling soil moisture state in detail over South Africa using the TOPKAPI hydrological model in LSM mode forced by rainfall and evapotranspiration estimates. This system is currently running as a "proof of concept" prototype.

We have compared the SSI simulations produced by TOPKAPI to surface soil moisture retrievals from the ASCAT instrument onboard the METOP polar orbiting satellite. The ASCAT soil moisture product is operationally disseminated for the European

region, but is not (yet) operationally available in Africa. We found a good correspondence between time filtered values of SSM averaged over 0.25° and 0.5° blocks for several climatic regions in South Africa, but found poor correspondence in the dry Western Cape site considered. The R^2 maps in Fig. 16 show that this is to be expected since the Western Cape site falls in the broad region of poor correspondence between the TOPKAPI and ASCAT estimates. These results are consistent with those found by Vischel et al. (2008b) for the Liebenbergsvlei catchment. In that earlier study we compared the soil moisture estimates obtained from a detailed catchment implementation of TOPKAPI (a network of laterally inter-connected cells) with the time filtered soil moisture product retrieved from ASCAT's predecessor onboard the ERS-1 and ERS-2 polar orbiters.

These results are encouraging as they suggest that there is a good possibility of improving the space time coverage of soil moisture as estimated by active microwave sensors on-board polar orbiting satellites, by using hydrological modelling (in LSM mode or in detail where required) and assimilating the information provided by microwave sensors (e.g. Crow and Ryu, 2009; Parajka et al., 2006). The resulting soil moisture field will be valuable for Flash Flood Guidance and other applications in the region.

Acknowledgements. The authors gratefully acknowledge the support of the South African Water Research Commision, which provided funding for this work.

References

Albergel, C., Rüdiger, C., Carrer, D., Calvet, J.-C., Fritz, N., Naeimi, V., Bartalis, Z., and Hasenauer, S.: An evaluation of ASCAT surface soil moisture products with in-situ observations in Southwestern France, Hydrol. Earth Syst. Sci., 13, 115–124, 2009, http://www.hydrol-earth-syst-sci.net/13/115/2009/. 7441

Allen, R., Pereira, L., Raes, D., and Smith, M.: Crop evapotranspiration – Guidelines for computing crop water requirements, FAO Irrigation and drainage paper, Rome, Tech. rep., 56, 1998. 7441, 7443, 7445, 7446, 7447, 7449

Allen, R., Pruitt, W., Wright, J., Howell, T., Ventura, F., Snyder, R., Itenfisu, D., Steduto, P., Berengena, J., Yrisarry, J., Smith, M., Pereira, L., Raes, D., Perrier, A., Alves, I., Walter, I., and Elliott, R.: A recommendation on standardized surface resistance for hourly calculation of reference ET_0 by the FAO56 Penman-Monteith method, Agr. Water Manage., 81, 1–22, 2006. 7446

Bartalis, Z., Naeimi, V., Hasenauer, S., and Wagner, W.: ASCAT Soil Moisture Product Handbook, ASCAT Soil Moisture Report Series, Tech. Rep. 15, Institute of Photogrammetry and Remote Sensing, Vienna University of Technology, Austria, 2008. 7442, 7450, 7455, 7456, 7482

Crow, W.: A Novel Method for Quantifying Value in Spaceborne Soil Moisture Retrievals, J. Hydrometeorol., 8, 56–67, 2007. 7441

Crow, W. T. and Ryu, D.: A new data assimilation approach for improving runoff prediction using remotely-sensed soil moisture retrievals, Hydrol. Earth Syst. Sci., 13, 1–16, 2009, http://www.hydrol-earth-syst-sci.net/13/1/2009/. 7457

Eisenhauer, J.: Regression through the origin, Teaching Statistics, 25, 76–80, 2003. 7446

Figa-Saldaña, J., Wilson, J., Attema, E., Gelsthorpe, R., Drinkwater, M., and Stoffelen, A.: The advanced scatterometer (ASCAT) on the meteorological operational (MetOp) platform: A follow on for European wind scatterometers, Can. J. Remote Sens., 28, 404–412, 2002. 7452, 7474

Gordon, H.: Errors in computer packages. Least squares regression through the origin, The Statistician, 30, 23–29, 1981. 7446

Guerschman, J., Dijk, A. V., Mattersdorf, G., Beringer, J., Hutley, L., Leuning, R., Pipunic, R., and Sherman, B.: Scaling of potential evapotranspiration with MODIS data reproduces flux observations and catchment water balance observations across Australia, J. Hydrol., 369, 107–119, 2009. 7449

Huffman, G., Adler, R., Bolvin, D., Gu, G., Nelkin, E., Bowman, K., Hong, Y., Stocker, E., and Wolff, D.: The TRMM Multi-satellite Precipitation Analysis: Quasi-global, multi-year, combined-sensor precipitation estimates at fine scale, J. Hydrometeorol., 8, 38–55, 2007. 7449

Kerr, Y., Waldteufel, P., Wigneron, J.-P., Martinuzzi, J.-M., Font, J., and Berger, M.: Soil moisture retrieval from space: The soil moisture and ocean salinity mission (SMOS), IEEE T. Geosci. Remote, 39, 1729–1735, 2001. 7441

Liu, Z. and Todini, E.: Towards a comprehensive physically-based rainfall-runoff model, Hydrol. Earth Syst. Sci., 6, 859–881, 2002, http://www.hydrol-earth-syst-sci.net/6/859/2002/. 7441
McCabe, M. and Wood, E.: Scale influences on the remote estimation of evapotranspiration using multiple satellite sensors, Remote Sens. Environ., 105, 271–285, 2006. 7442
Midgley, D., Pitman, W., and Middleton, B.: Surface Water Resources of South Africa 1990, Water Research Commission Report, Tech. rep. No. 298/94, 1994. 7451, 7470
Naeimi, V., Bartalis, Z., and Wagner, W.: ASCAT Soil Moisture: An Assessment of the Data Quality and Consistency with the ERS Scatterometer Heritage, J. Hydrometeorol., 10, 555–563, 2009. 7455
Njoku, E., Jackson, T., Lakshmi, V., Chan, T., and Nghiem, S.: Soil moisture retrieval from AMSR-E, IEEE T. Geosci. Remote, 41, 215–229, 2003. 7441
Ntelekos, A., Georgakakos, K., and Krajewski, W.: On the Uncertainties of Flash Flood Guidance: Toward Probabilistic Forecasting of Flash Floods, J. Hydrometeorol., 7, 271–285, 2006. 7441
Parajka, J., Naeimi, V., Blöschl, G., Wagner, W., Merz, R., and Scipal, K.: Assimilating scatterometer soil moisture data into conceptual hydrologic models at the regional scale, Hydrol. Earth Syst. Sci., 10, 353–368, 2006, http://www.hydrol-earth-syst-sci.net/10/353/2006/. 7457
Pfeffer, J.: Evaluation of remote sensing soil water products by intercomparison over South Africa, Master's thesis, Sciences de la Terre, de l'Univers et de l'Environnement, Université Joseph Fourier de Grenoble, France, 2008. 7451
Savage, M.: Estimation of evaporation using a dual-beam surface layer scintillometer and component energy balance measurements, Agr. Forest Meteorol., 149, 501–517, 2009. 7445
Savage, M., Everson, C., and Metelerkamp, B.: Bowen ratio evaporation measurement in a remote montane grassland: Data integrity and fluxes, J. Hydrol., 376, 249–260, 2009. 7445
Scipal, K., Scheffler, C., and Wagner, W.: Soil moisture-runoff relation at the catchment scale as observed with coarse resolution microwave remote sensing, Hydrol. Earth Syst. Sci., 9, 173–183, 2005, http://www.hydrol-earth-syst-sci.net/9/173/2005/. 7441
Su, Z.: The Surface Energy Balance System (SEBS) for estimation of turbulent heat fluxes, Hydrol. Earth Syst. Sci., 6, 85–100, 2002, http://www.hydrol-earth-syst-sci.net/6/85/2002/. 7442

Tasumi, M., Allen, R., Trezza, R., and Wright, J.: Satellite-Based Energy Balance to Assess Within-Population Variance of Crop Coefficient Curves, J. Irrig. Drain. E.-ASCE, 131, 94–109, 2005. 7447

Vischel, T., Pegram, G., Sinclair, S., and Parak, M.: Implementation of the TOPKAPI model in South Africa: Initial results from the Liebenbergsvlei catchment, Water SA, 34, 1–12, 2008a. 7441, 7449

Vischel, T., Pegram, G. G. S., Sinclair, S., Wagner, W., and Bartsch, A.: Comparison of soil moisture fields estimated by catchment modelling and remote sensing: a case study in South Africa, Hydrol. Earth Syst. Sci., 12, 751–767, 2008b. 7441, 7457

Wagner, W., Lemoine, G., and Rott, H.: A Method for Estimating Soil Moisture from ERS Scatterometer and Soil Data, Remote Sens. Environ., 70, 191–207, 1999. 7441, 7451

Wagner, W., Bloschl, G., Pampaloni, P., Calvet, J.-C., Bizzarri, B., Wigneron, J.-P., and Kerr, Y.: Operational readiness of microwave remote sensing of soil moisture for hydrologic applications, Nord. Hydrol., 38, 1–20, 2007. 7450

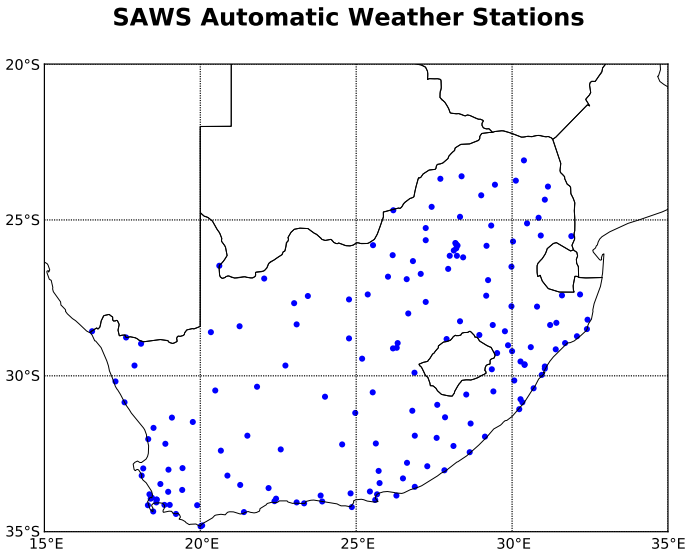

Fig. 1. Plot showing the locations of the South African Weather Services (SAWS) current automatic weather stations. Other meteorological stations exist, but are either manually read, or are operated by different organizations. The coverage is sparse, with only 164 stations in 1.2 million km^2.

HESSD
6, 7439–7482, 2009

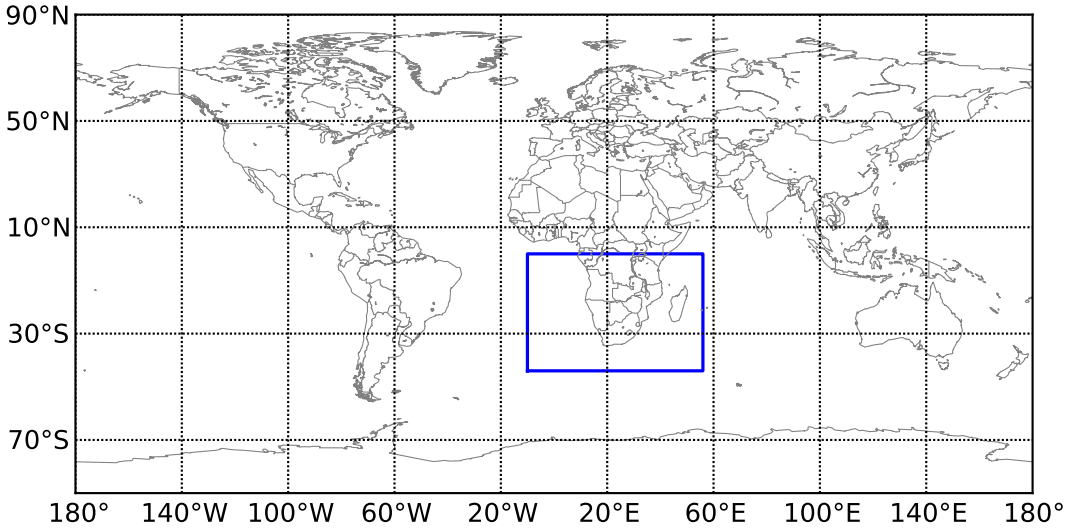

Fig. 2. Bounding region for the SAWS Unified Model runs. The blue box on the map shows the extent of the region modelled by SAWS.

HESSD
6, 7439–7482, 2009

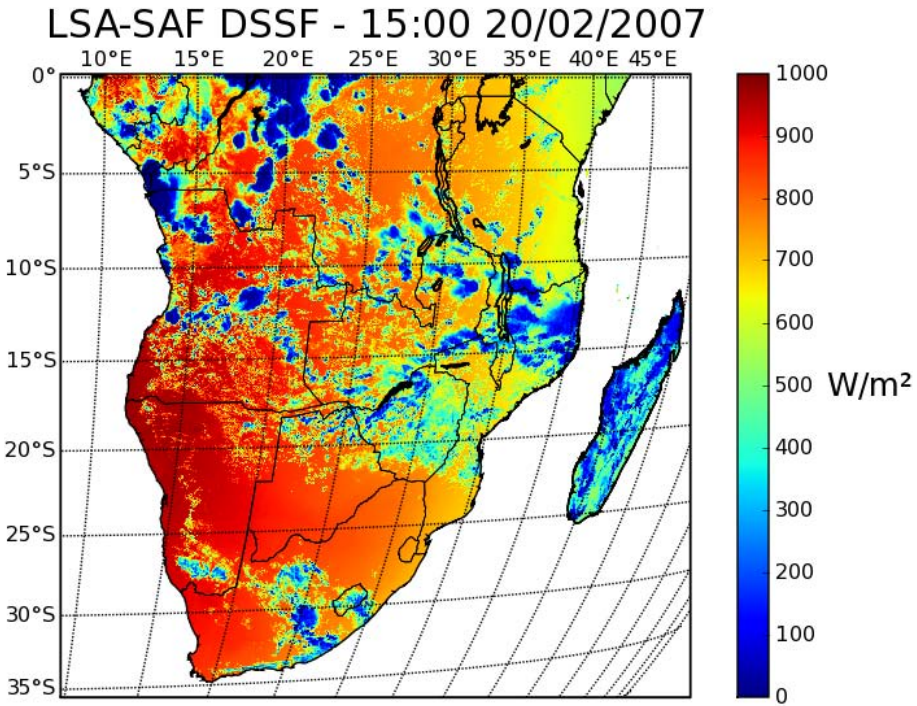

Fig. 3. Example of the LSA-SAF DSSF product for Southern Africa. The data are available at half hour intervals, via the EUMETCast system.

HESSD

6, 7439–7482, 2009

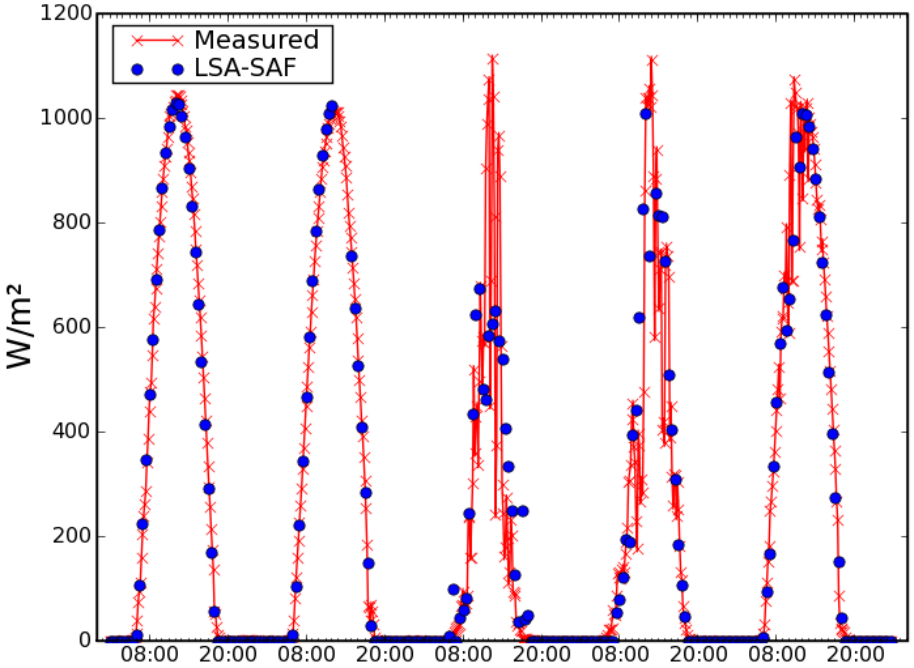

Fig. 4. Comparison of observed solar radiation with observations in KwaZulu-Natal, South Africa made by the CSIR (C. Everson, 2008, personal communication). The blue points are the half-hourly DSSF estimates from the LSA-SAF product and the red crosses are the data observed at the ground, measured at 12 min intervals.

HESSD
6, 7439–7482, 2009

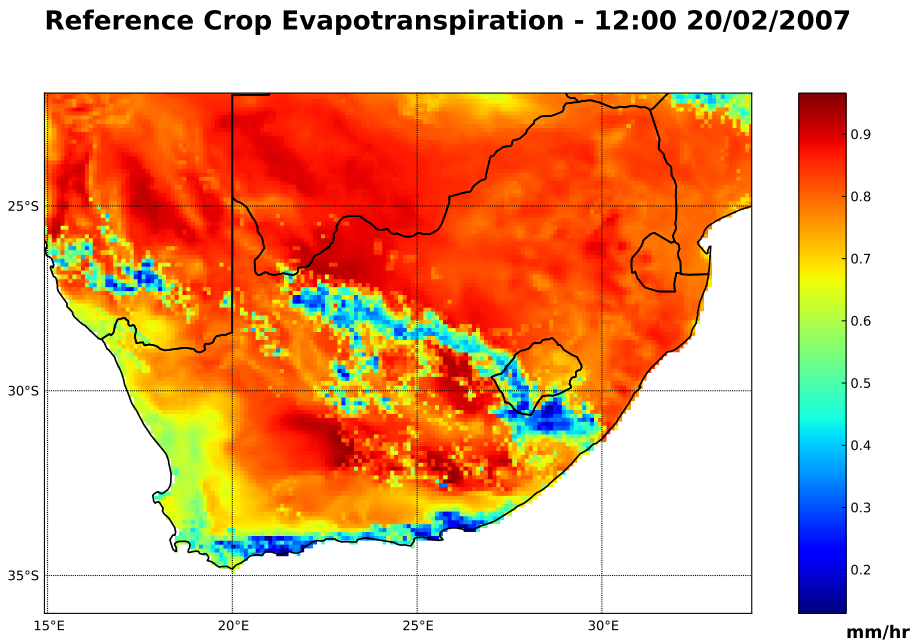

Fig. 5. An hourly estimate of ET_0 computed from NWP forecast data and LSA-SAF radiation estimates.

HESSD
6, 7439–7482, 2009

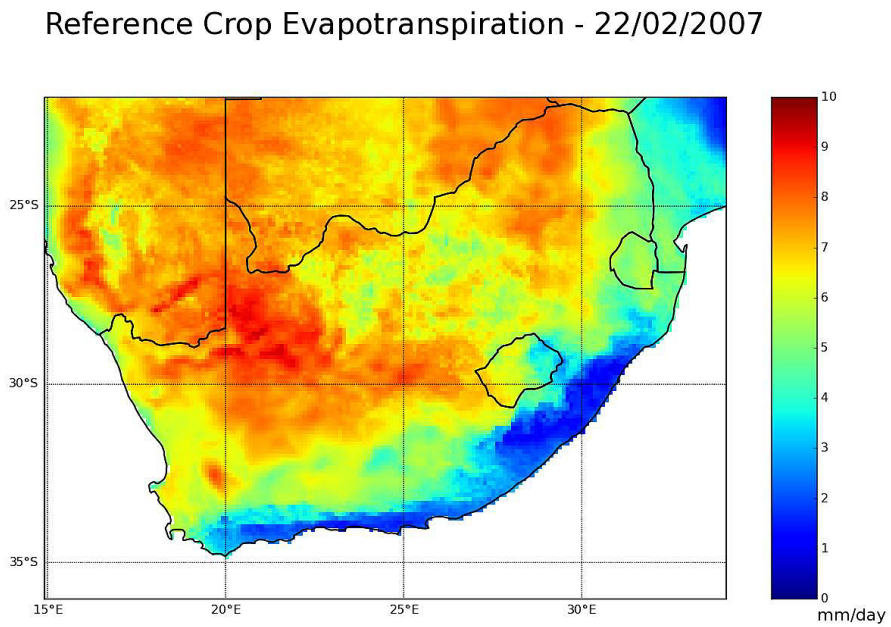

Fig. 6. Daily total of ET_0 computed by summing hourly estimates based on NWP forecast data and LSA-SAF radiation estimates.

HESSD

6, 7439–7482, 2009

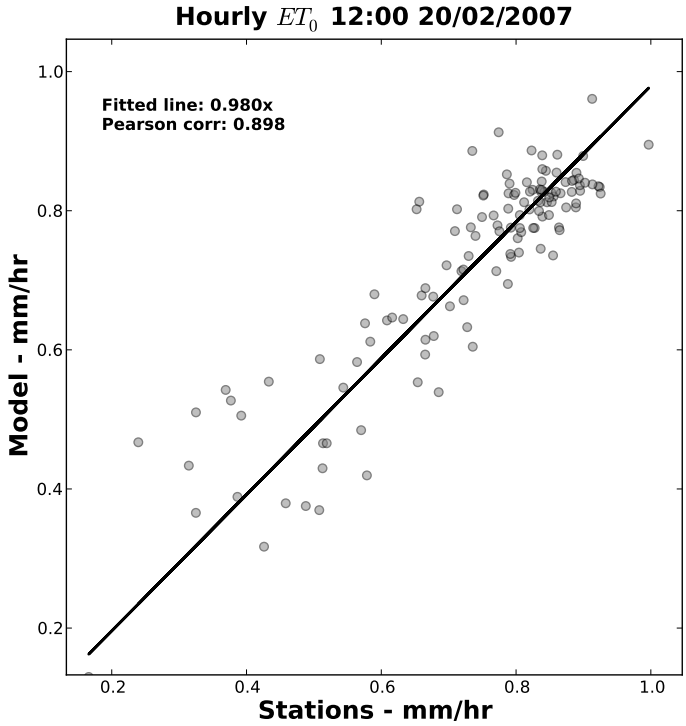

Fig. 7. A typical regression between hourly totals of ET_0 computed from forecast model data and observed meteorological parameters at 164 automatic weather stations (Fig. 1).

HESSD
6, 7439–7482, 2009

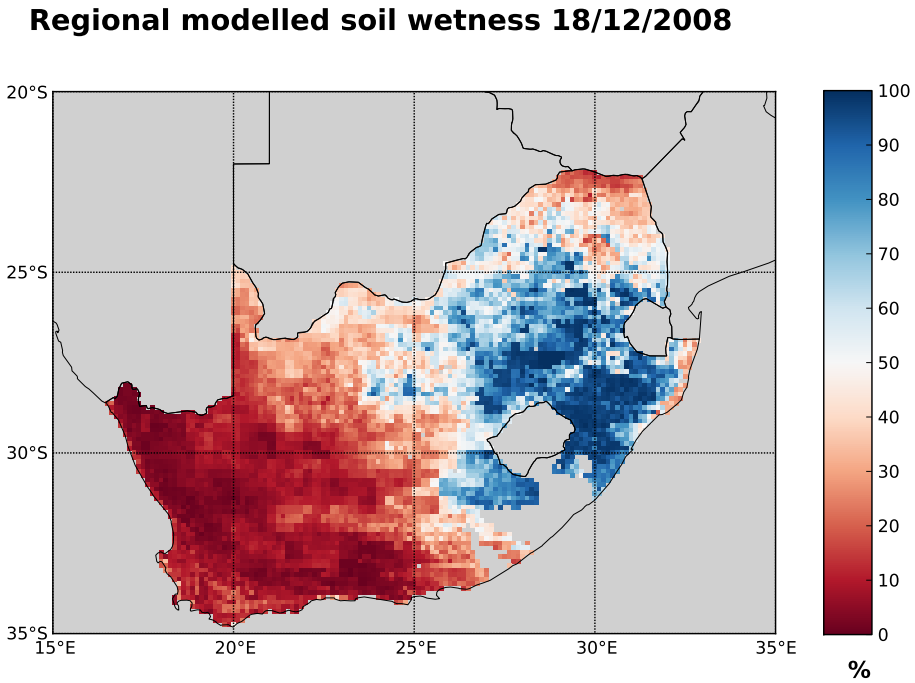

Fig. 8. An example of the country-wide soil moisture estimates produced by TOPKAPI in LSM mode. The colour scale represents SSI, the percentage of soil void space filled by water (see Eq. 5).

HESSD
6, 7439–7482, 2009

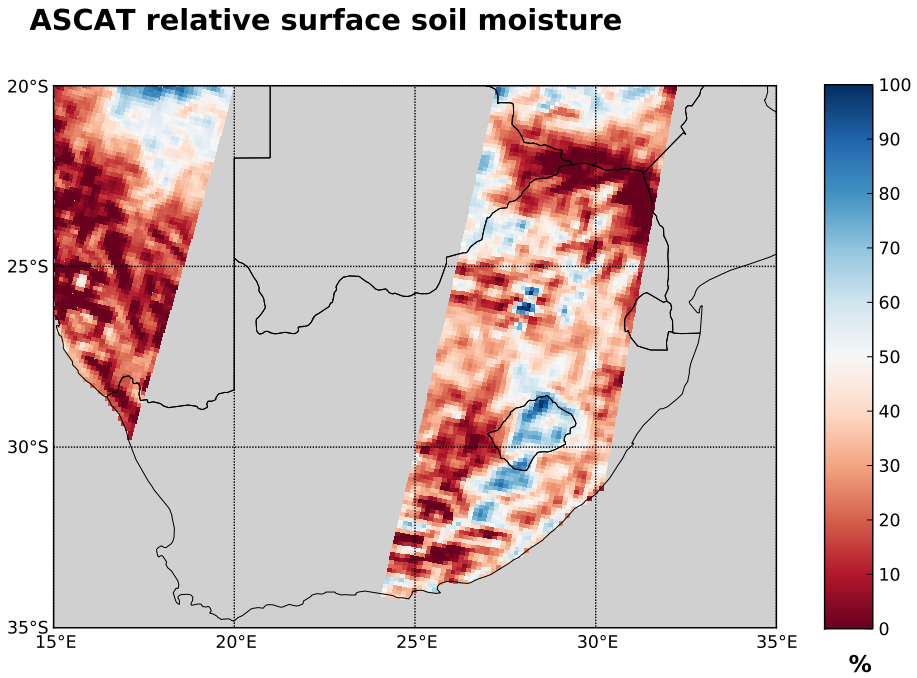

Fig. 9. Relative surface soil moisture (SSM) retrieval from ASCAT. The satellite overpass time is approximately eight hours after the TOPKAPI-LSM SSI estimates shown in Fig. 8.

HESSD
6, 7439–7482, 2009

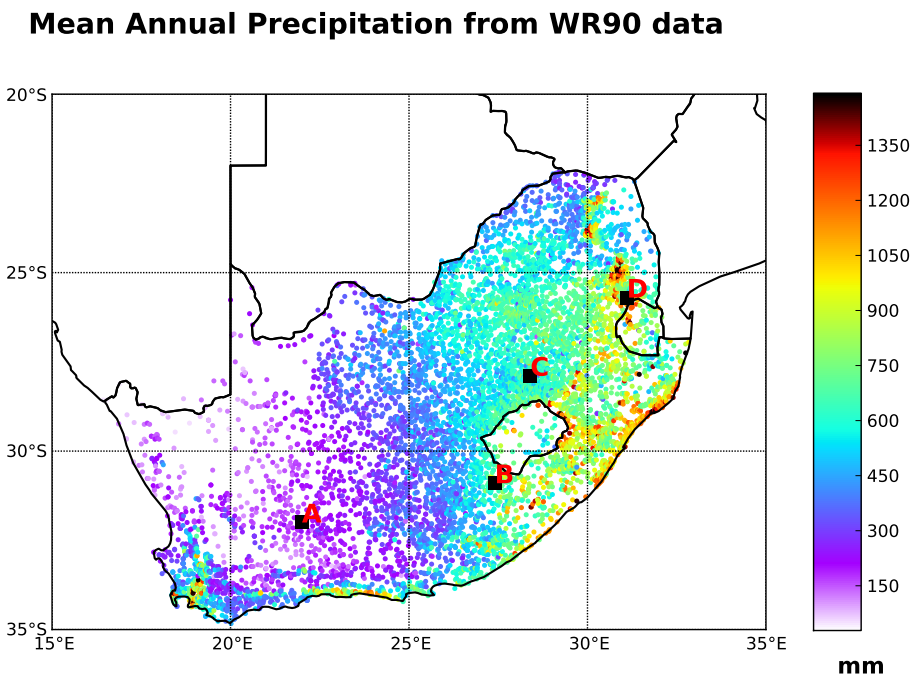

Fig. 10. Locality of the four different regions considered, plotted over MAP data obtained from WR90 (Midgley et al., 1994). The general trend is for MAP to increase from West to East. An important exception is the southern coastline, which receives significant winter rainfall associated with frontal systems.

HESSD
6, 7439–7482, 2009

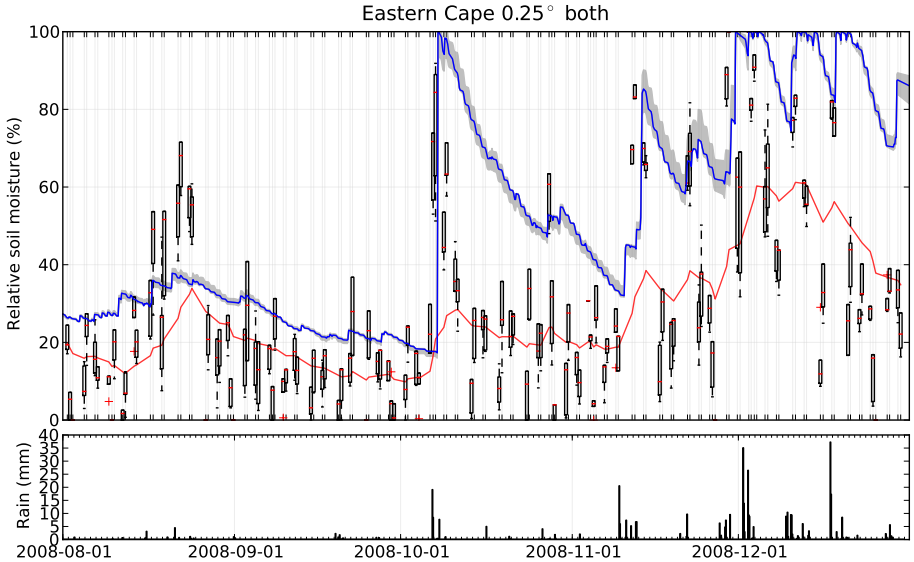

Fig. 11. TOPKAPI-LSM and ASCAT derived soil wetness, and TRMM 3B42RT 3 h accumulated rainfall. The top panel shows the median TOPKAPI-LSM SSI averaged over a 0.25° block (blue line), with the inter-quartile range of these four estimates within the block shown by the grey fill. The range of ASCAT estimates (they number between 2 and 6 on a given day in a 0.25° square) within the box at each overpass time is shown by the box and whisker plots (for ascending and descending orbits), while the red line shows the filtered time series of the mean ASCAT estimates. The bottom panel shows a histogram of 3 h rainfall accumulations.

HESSD
6, 7439–7482, 2009

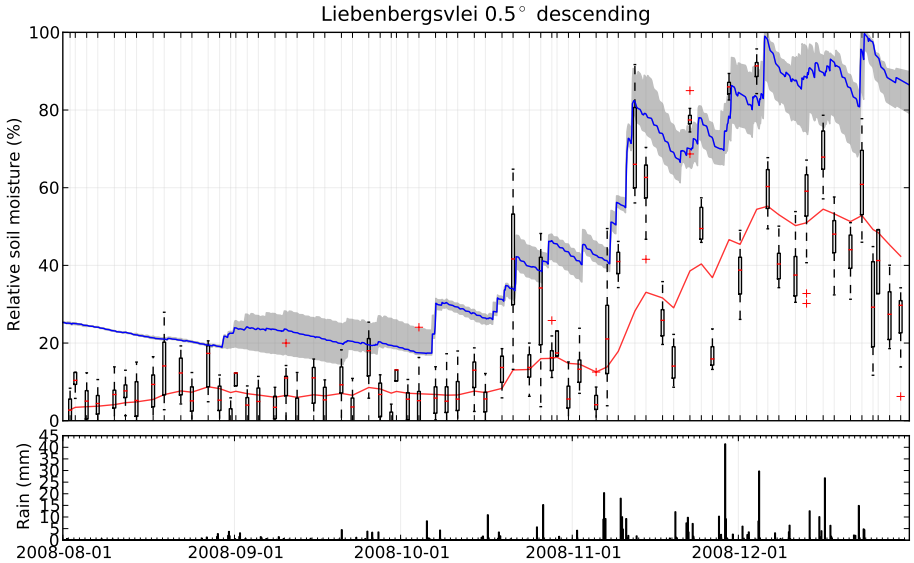

Fig. 12. TOPKAPI-LSM and ASCAT derived soil wetness, and TRMM 3B42RT 3 h accumulated rainfall. The top panel shows the median TOPKAPI-LSM SSI averaged over a 0.25° block (blue line), with the inter-quartile range of these four estimates within the block shown by the grey fill. The range of ASCAT estimates (they number between 2 and 6 on a given day in a 0.25° square) within the box at each overpass time is shown by the box and whisker plots (for ascending and descending orbits), while the red line shows the filtered time series of the mean ASCAT estimates. The bottom panel shows a histogram of 3 h rainfall accumulations.

HESSD
6, 7439–7482, 2009

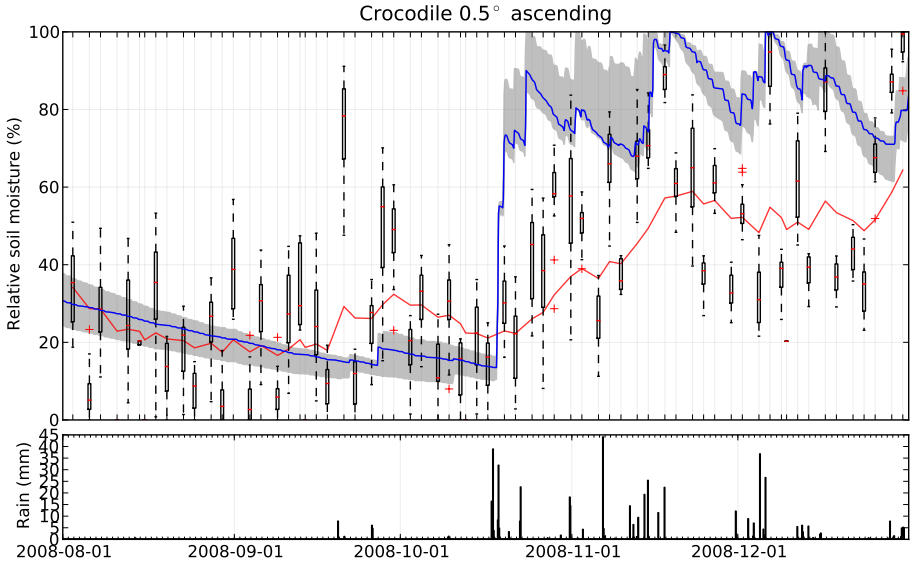

Fig. 13. TOPKAPI-LSM and ASCAT derived soil wetness, and TRMM 3B42RT 3 h accumulated rainfall. The top panel shows the median TOPKAPI-LSM SSI averaged over a 0.25° block (blue line), with the inter-quartile range of these four estimates within the block shown by the grey fill. The range of ASCAT estimates (they number between 2 and 6 on a given day in a 0.25° square) within the box at each overpass time is shown by the box and whisker plots (for ascending and descending orbits), while the red line shows the filtered time series of the mean ASCAT estimates. The bottom panel shows a histogram of 3 h rainfall accumulations.

HESSD
6, 7439–7482, 2009

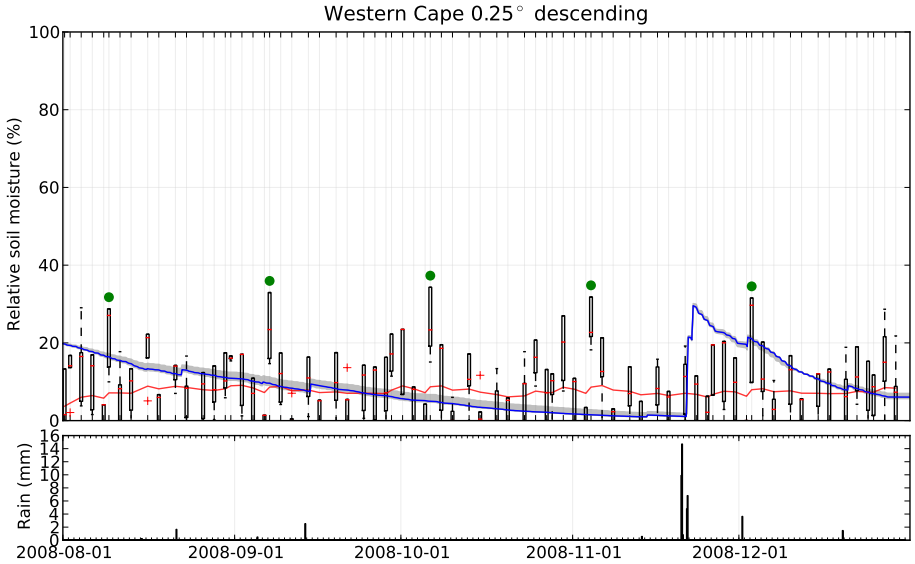

Fig. 14. TOPKAPI-LSM and ASCAT derived soil wetness, and TRMM 3B42RT 3 h accumulated rainfall. The top panel shows the median TOPKAPI-LSM SSI averaged over a 0.25° block (blue line), with the inter-quartile range of these four estimates within the block shown by the grey fill. The range of ASCAT estimates (they number between 2 and 6 on a given day in a 0.25° square) within the box at each overpass time is shown by the box and whisker plots (for ascending and descending orbits), while the red line shows the filtered time series of the mean ASCAT estimates. The bottom panel shows a histogram of 3 h rainfall accumulations. The sequence of green dots highlight a marked increase in the ASCAT estimated soil moisture, which has a periodicity that matches the 29 day repeat cycle of MetOp (Figa-Saldaña et al., 2002).

HESSD
6, 7439–7482, 2009

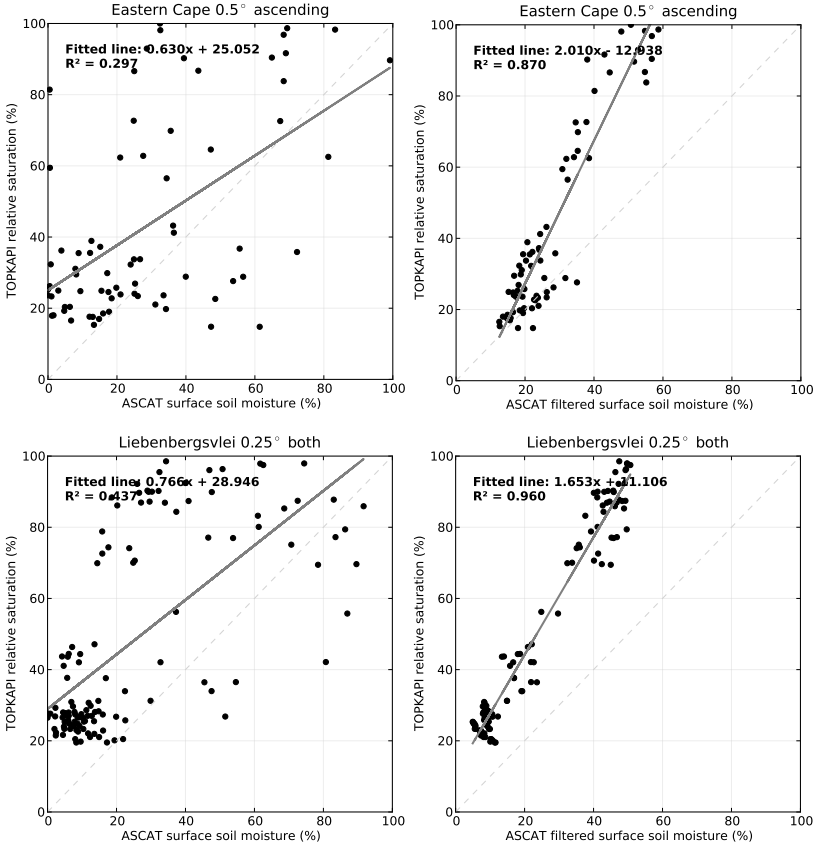

Fig. 15. Scatter plots of the block mean ASCAT soil moisture and closest (in time) block mean TOPKAPI SSI, showing the fitted linear regression line and R^2 values.

HESSD
6, 7439–7482, 2009

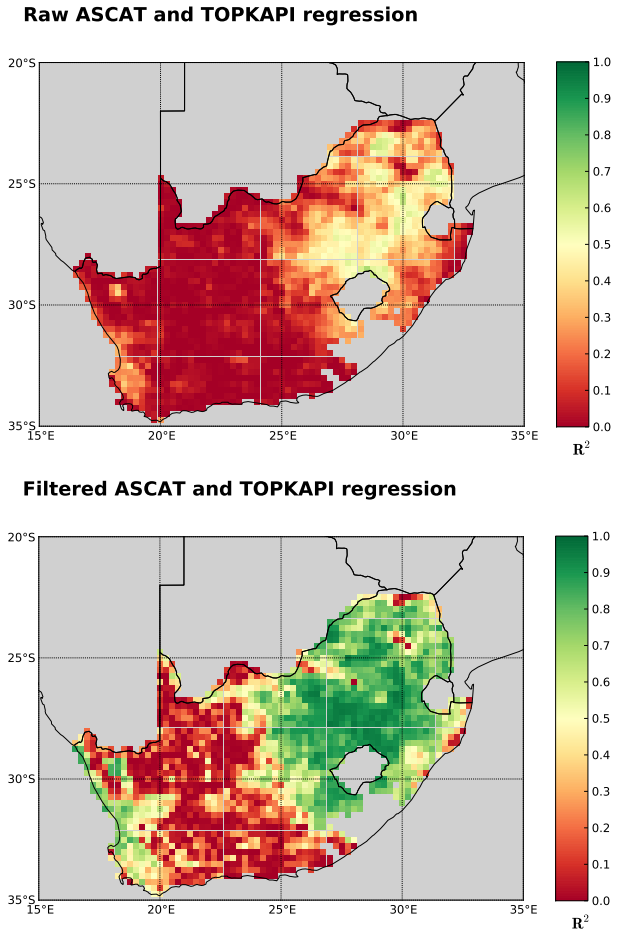

Fig. 16. Maps of R^2 computed for the block mean (0.25°) ASCAT soil moisture and closest (in time) block mean TOPKAPI-LSM SSI – the upper and lower panels show the SSI comparisons against unfiltered and filtered ASCAT SSM estimates, respectively.

HESSD
6, 7439–7482, 2009

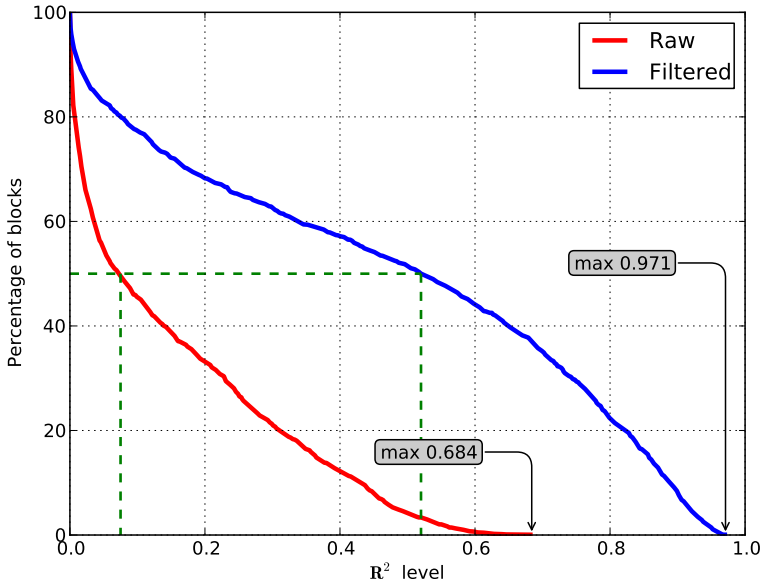

Fig. 17. Percentage of 0.25° blocks analysed that have an R^2 greater than or equal to the value shown on the x-axis. The green dashed lines indicate the R^2 level which is equalled or exceeded in 50% of the blocks.

HESSD
6, 7439–7482, 2009

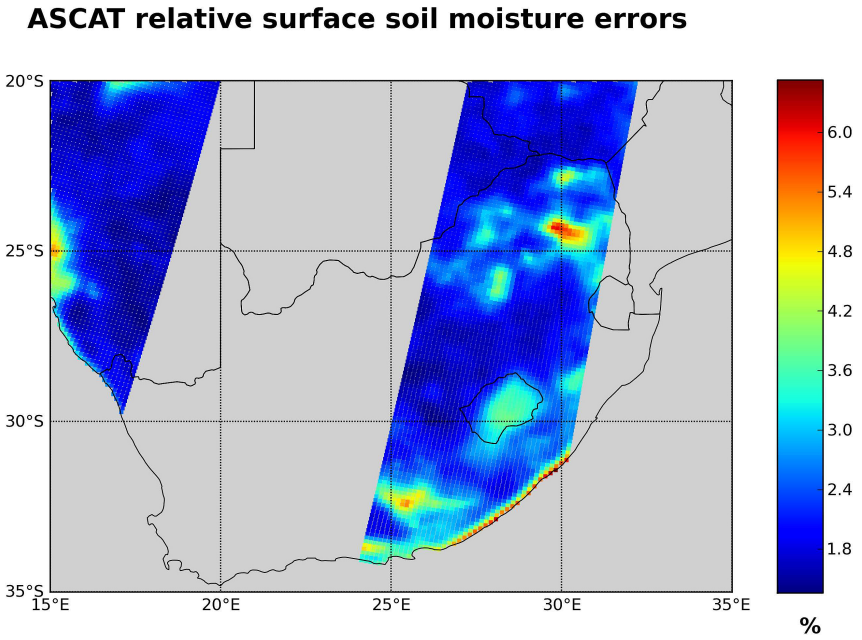

Fig. 18. Estimated error of the relative surface soil moisture retrieval from ASCAT. The satellite overpass matches that shown in Fig. 9.

HESSD
6, 7439–7482, 2009

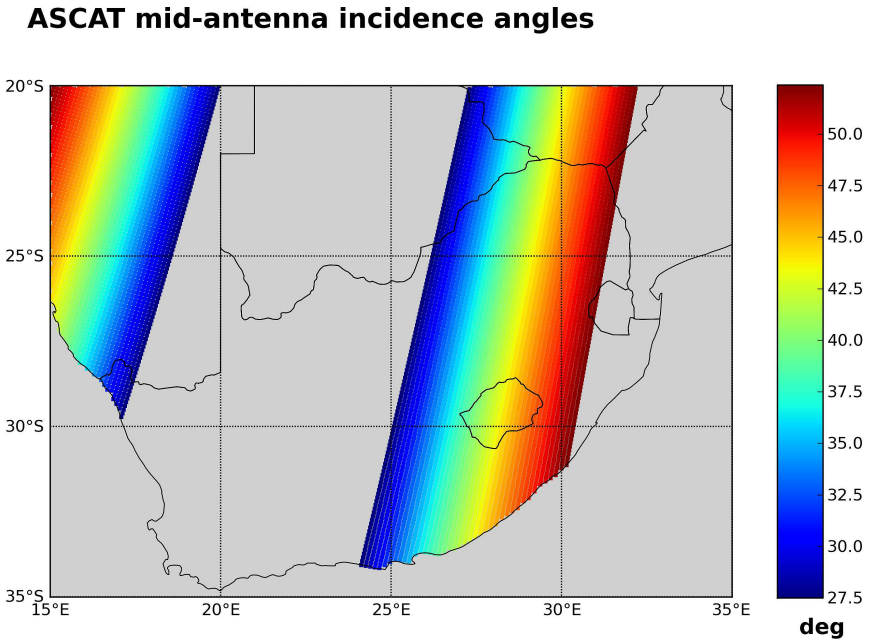

Fig. 19. Incidence angle (in decimal degrees) for the middle antenna of the ASCAT instrument. The satellite overpass time matches that shown in Fig. 9.

HESSD
6, 7439–7482, 2009

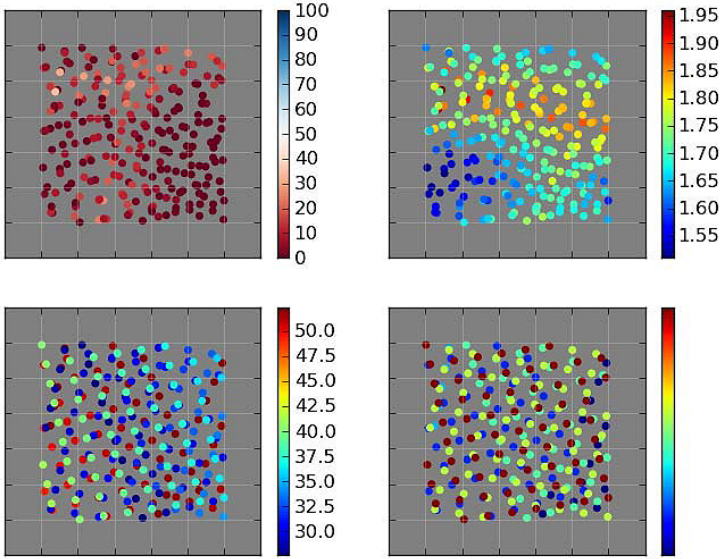

Fig. 20. Scatter plot of ASCAT information for the western cape site on a 0.5° block over a 5 day period (4 overpasses). Top left is SSM in percentage. Top right is reported SSM error in percentage. Bottom left is mid antenna incidence angles. Bottom right is time of overpass.

HESSD
6, 7439–7482, 2009

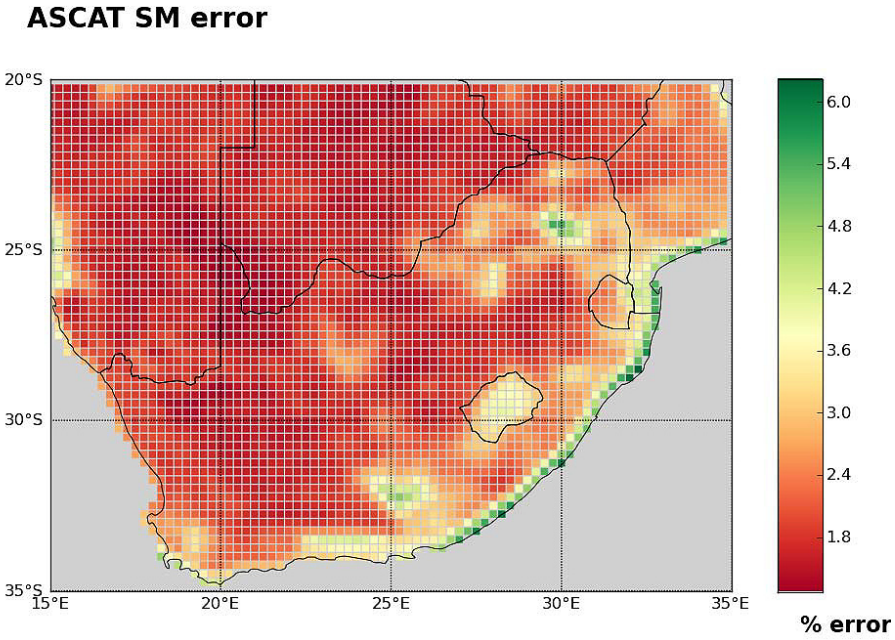

Fig. 21. Five month spatially averaged SSM error estimate provided with the ASCAT product. The reported error estimates have been averaged over 0.25° blocks for each overpass and the time average for each block calculated.

HESSD
6, 7439–7482, 2009

The Soil Moisture Retrieval Method

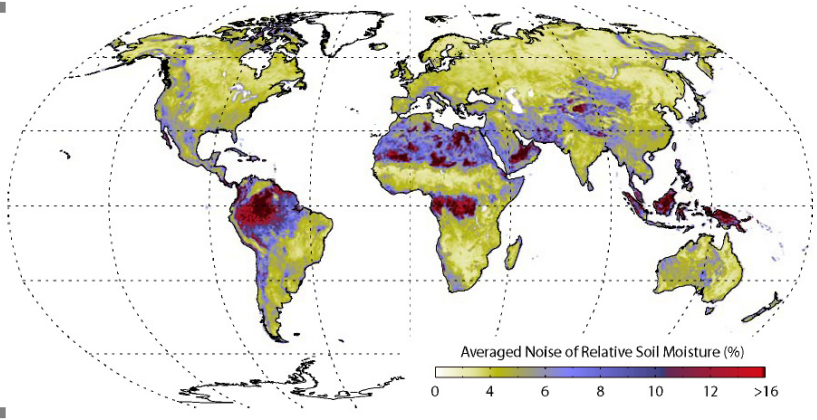

Figure 3-4

Average of the estimated soil moisture noise.

Fig. 22. Yearly average of ERS based surface soil moisture retrievals. Taken from Bartalis et al. (2008). The broad patterns shown over South Africa, match those shown in Fig. 16, which shows the correlation computed between ASCAT SSM and TOPKAPI SSI.

HESSD

6, 7439–7482, 2009